processes

MDPI

Article

Recovery of Rare-Earth Elements from Printed Circuit Boards by Vacuum Pyrolysis and Multiple Electrostatic Separation

Andjelka Popović [1], Vaso Manojlović [2,*], Borivoj Adnadjević [3], Jelena Petrović [4], Željko Kamberović [2] and Milisav Ranitović [5]

[1] Faculty of Technology Novi Sad, University of Novi Sad, Bulevar Cara Lazara 1, 21000 Novi Sad, Serbia; anzelikapopovic@gmail.com
[2] Faculty of Technology and Metallurgy, University of Belgrade, Karnegijeva 4, 11120 Belgrade, Serbia; kamber@tmf.bg.ac.rs
[3] Faculty of Physical Chemistry, University of Belgrade, Studentski trg 12–16, 11102 Belgrade, Serbia; adnadjevic@mts.rs
[4] Mining and Metallurgy Institute Bor, Zeleni Bulevar 35, 19210 Bor, Serbia; jelena.petrovic@irmbor.co.rs
[5] Innovation Center of the Faculty of Technology and Metallurgy LTD in Belgrade, Karnegijeva 4, 11000 Belgrade, Serbia; mranitovic@tmf.bg.ac.rs
* Correspondence: v.manojlovic@tmf.bg.ac.rs

Abstract: The influence of the multi-stage electrostatic separation (ESS) of mechanically treated and magnetically separated waste electronic material and the pyrolysis of the selected ESS fraction on the distribution of metal elements (MEs), elements contained in refractory oxides (EROs), bromine (Br), and rare-earth elements (REEs) contained in waste electronic material was studied. The concentration of MEs, Br, and EROs in the tested samples was determined by X-ray fluorescence analysis, and the concentration of REEs and uranium was determined by inductively coupled plasma mass spectrometry (ICP-MS). The analysis of the distribution of elements during the multi-stage ESS showed that MEs were predominantly distributed in the conductive fraction and Br, EROs, and REEs were distributed in the nonconductive fraction. The nonconductive fraction (NC2) of the two-stage ESS was subjected to a low-temperature vacuum pyrolysis (T = 550 °C, p = 10 mbar). The distribution of pyrolysis products of the NC2 fraction was determined. The main products of the vacuum pyrolysis experiments were the solid residue phase (54.4 wt.%) and oils (35.4 wt.%). It has been proven that pyrolysis can significantly increase the concentration of MEs, EROs, and REEs in raw materials, thereby providing a method for cost-effectively obtaining of REEs from waste printed circuit boards.

Keywords: waste printed circuit boards (WPCBs); rare-earth elements (REEs); electrostatic separation (ESS); low-temperature vacuum pyrolysis

check for updates

Citation: Popović, A.; Manojlović, V.; Adnadjević, B.; Petrović, J.; Kamberović, Ž.; Ranitović, M. Recovery of Rare-Earth Elements from Printed Circuit Boards by Vacuum Pyrolysis and Multiple Electrostatic Separation. *Processes* **2022**, *10*, 1152. https://doi.org/10.3390/pr10061152

Academic Editors: Paolo Trucillo, Amedeo Lancia, Francesco Di Natale and Izabela Czekaj

Received: 30 April 2022
Accepted: 3 June 2022
Published: 8 June 2022

Publisher's Note: MDPI stays neutral with regard to jurisdictional claims in published maps and institutional affiliations.

Copyright: © 2022 by the authors. Licensee MDPI, Basel, Switzerland. This article is an open access article distributed under the terms and conditions of the Creative Commons Attribution (CC BY) license (https://creativecommons.org/licenses/by/4.0/).

1. Introduction

Rare-earth elements make up a group of 17 elements (15 lanthanoids, with atomic numbers 57–71), scandium (atomic number 21), and yttrium (atomic number 39) [1–6]. The chemical properties of REEs and their compounds are very similar as a consequence of similar electronic configuration [6]. Due to their unique atomic structures, and chemical, magnetic, optical, and luminescent properties, [6] REEs are widely used in the production of rechargeable batteries, autocatalytic converters, super magnets, LED bulbs, fluorescent materials, solar panels, etc. [1]. It is estimated that by the year 2025, total REEs consumption will reach 250 thousand tons/year, which represents 37% of the world's REEs reserves [7]. There are more than 250 REEs-bearing minerals, but most of the global REEs production is provided via bastnaesite and monazite, along with xenotime [5]. China dominates the global supply of REEs with about 60% of the world's total light oxide-equivalent REEs [8]. At the same time, China is the largest consumer of REEs [9].

According to data provided by the Global E-waste Monitor 2020, 53.6 million tons of WEEEs were produced in 2019, giving a prospect to recover metals with a combined value

of USD 57 billion. WEEE volumes are growing from year to year at an alarming annual growth rate of 3–5%, and it is estimated that by 2030, 74 million tons will be generated. It is worrying that only 1/5 of the total WEEE generated is recycled, and for the remaining 44.3 million tons, it is not known exactly where it ends up [10]. Waste printed circuit boards (WPCBs) are valuable components of WEEEs that make up about 3–6% of the total weight of WEEEs [11]. WPCBs consist of about 40:30:30 of metal, plastic, and refractory oxides (ROs), respectively [12–14]. The nonmetallic fraction includes reinforcing materials, thermosetting resins, brominated flame retardants (BFRs), and other additives [15,16]. The WPCBs analysis of various electronic devices detected 56 elements: 14 rare-earth elements, six platinum group metals, 20 critical metals, and 16 other elements, including some precious metals [17]. WPCBs contain over 40% of valuable metals (20% copper, 1000 ppm silver, 250 ppm gold, 110 ppm palladium, and 95.88 ppm REEs) [18]. According to statistics, the global recycling rate of REEs is less than 1% [19,20].

Despite the great theoretical and practical significance, there is a relatively small number of scientific papers in which the possibility of obtaining REEs from waste materials has been examined. In order to produce REEs and rare-earth oxides (RE_2O_3) from natural ores and concentrates, several hydrometallurgical and pyrometallurgical methods were developed [21], such as dry digestion [22], the acid baking process [23], and carbothermal reduction [24]. A comprehensive review of hydrometallurgical methods for obtaining REEs and RE_2O_3 was given in the study of Zhang et al. [25] and the study of Kaya et al. [21]. The methods mainly included selective or complete leaching of REEs followed by precipitation [26], solvent extraction, or the ionic liquids extraction process [27]. The production of REEs from ores and concentrates leads to several environmental problems [21,23]. The recovery of REEs from waste materials is critical for ensuring the sustainability for the production of REEs [2].

The great need to find an efficient method for WPCBs recycling has led to pyrolysis, an alternative energy-intensive but environmentally friendly method. Pyrolysis was shown to be a viable alternative to treat the nonmetallic fraction of WPCBs for resource recovery and causing less environmental problems associated with the final products [28]. Pyrolysis is a process in which resins from WPCBs are converted into flammable gases and tar, which can be used as a fuel for the pyrolysis process itself, while metals and glass remain as residues, which may be further recycled by the hydrometallurgical process [29]. Khanna et al. (2018) [30] emphasized the high affinity of several REEs for the nonmetallic fraction of the pyrolytic residue. Khanna et al. (2019) [31] processed tests on different WPCBs by pyrolysis at a temperature (850 °C) for 15 min in a pyrolysis furnace. Pyrolysis residues were separated into a metal fraction (Cu, Pb, Sn) and nonmetal fraction with (slag, or glass, ceramic, and carbon). It was found that REEs were concentrated in the nonmetallic fraction and contained Pr, Nd, La, Ce, I, and Di.

REEs are distributed in different fractions of mechanical separation, so it is essential to find an economically feasible method of concentrating REEs in one of the fractions. The metallic fraction is treated with metallurgical processes, which usually end with the electrowinning of the basic metal (e.g., copper), after which REEs are concentrated and can be recovered from the sludge. Generally, the nonconductive fraction can be recycled to produce polymers, but the nonmetallic dusty fraction is neglected and is considered in the literature as non-recyclable. This fact led us to propose a low-temperature vacuum pyrolysis process combined with minimal mechanical pretreatment as an environmentally friendly and economically feasible way to concentrate REEs from WPCBs in the pre-treatment step. Through a combination of mechanical separation methods and vacuum pyrolysis methods, we aim to quantitatively determine the element distribution and concentration of REEs. The concentration of REEs in a non-conductive dusty phase is suitable for further processing and recycling. Considering the above, the main objectives of this paper are:

(a) Examination of the influence of multistage ESS on the distribution of MEs, Br, EROs, and REEs by the obtained fractions;

(b) Selection of ESS fraction for pyrolytic transformation to obtain metallic-nonmetallic phase and concentrating REEs;
(c) Determining the influence of low-temperature vacuum pyrolysis on the distribution and chemical composition of pyrolysis products.

2. Materials and Methods

2.1. Material

A sample of waste printed circuit boards (WPCBs) was obtained from the company "Alkemica Solutions", Novi Sad, Serbia. The WPCBs were a 100 kg mixture of 80% printed circuit board (PCB) (Intel—Unimicron Technology Corporation Taiwan, Taoyuan, Taiwan; Asus—computer Taipei, Taiwan; IBM—New York, NY, USA, etc.), 10% laptops, and 10% mobile phones (Chinese unlabeled production). WPCBs were not washed with water, nor were electronic components (processors, memory modules, control circuits, and chips) removed.

2.2. Mechanical Processing of Materials

Mechanical processing of materials included the following technological operations: crushing, grinding, and magnetic material separation. Crushing of materials was performed on a ball mill manufactured by "EMARK"—TURKEY, whose basic technical characteristics were the following: power of 11 kW; piece size up to ~(2 × 2 or 2 × 3) cm. Grinding of the material was performed on a mill with knives manufactured by "EMARK"—TURKEY, with the following basic technical characteristics: power of 30 kW; piece size up to <3 mm. Magnetic separation of materials was performed on the vibro table "EMARK"—TURKEY, with the following basic technical characteristics: power of 30 kW connected to an 8-bar compressor.

2.3. Electrostatic Separation of Materials

Electrostatic separation was performed using the "Hamos" Germany, model KWS-L, (Hamos GmbH, recycling-und Separationstechnik, Penzberg, Germany) with the following basic technical characteristics: separator electricity consumption of 3 kW/h, voltage of 35,000 V, drum speed of 2900 r/min, and charge between electrodes of 0 to 30 kV. The material was separated into three fractions: conductive (C), nonconductive (NC), and mixed (M).

2.4. Calculation of Weight Fraction in Electrostatic Separation Products

Calculating the weight concentration fraction of ESS fractions was performed by the gravimetric method—measuring the weight yield of each fraction.

2.5. Determination of Particle Size Distribution of Investigated Samples

The particle size distribution of fractions C1, M1, NC1, C2, M2, and NC2 was determined by the sieving method using the ASTM Retsch Vibratory Sieve Shaker AS 200 (Verder Scietific Headquarters, Haan, Germany) equipped with a standard set of sieves.

2.6. Determination of Bulk Density of Tested Samples

Determination of the bulk density of investigated samples, C1, M1, NC1, C2, M2, NC2, was performed according to the standard SRPS EN ISO 17828/2016.

2.7. Scanning Electron Microscopy (SEM)

Scanning electron microscopy (SEM) images were obtained on the Tescan MIRA3 XMU FESEM (TESCAN, Brno, Czech Republic), with the electron energies of 20 kV, in a high vacuum. Before the analysis, the samples were coated with a thin layer of Au using a standard sputtering technique (Polaron SC502Sputter Coater, Fison Instruments, Glasgow, UK).

2.8. Determination of the Chemical Composition of the Investigated Samples

Determination of the chemical composition of the investigated samples (raw materials, fraction after electrostatic separation, and metallic-nonmetallic fraction of pyrolysis elements) was performed by a X-ray fluorescence.

The XRF spectra of the raw materials, the fraction after electrostatic separation, and the metallic-nonmetallic fractions of the pyrolysis fraction were recorded on a model JSX-1000S X-ray fluorescence spectrometer (XRF) manufactured by JEOL, Freising, Germany.

XRF spectrum recording conditions were as follows: X-ray tube voltage of 50 kV, energy range of 0–41 kV, air scan, X-ray tube currents of 0.030 mA, collimator of 9.000 mm, open filter, PHA model T2, scan time from 60 to 90 s, number of steps per second from 199,071 to 365,555, and Δ3X (three measurements).

2.9. Determination of the Concentration of Elements from the REE Group in the Tested Samples

Determination of the concentration of elements, where the elements were from the REE group, was performed by the atomic absorption method (AAS).

Preparation of the samples for AAS recordings was performed by microwave digestion on a microwave device manufactured by "ETHOS".

The procedure for the preparation of a sample for analysis was as follows: weigh 0.1 g of the sample into a 50 mL Erlenmeyer flask, add 8 mL of the hydrochloric and nitric acids mixture (HCl + HNO_3 ratio 3:1), cool, perform the first digestion at 220 °C for 15 min, cool the sample, and add 2 mL of HF acid to the cooled sample, after which the second digestion is performed at a temperature of 220 °C for 20 min. The sample is cooled, and when cooled, it is added to 20 mL of boric H_3BO_3 acid to completely remove fluoride, after which the sample is cooled and diluted to a volume of 50 mL. The sample prepared in this way is further analyzed. The Ore Research and Exploration Pty Ltd. (Bayswater North, Australia) Assay Standard (OREAS 924) was used to verify the accuracy of the results (three measurements) Δ3X.

The Degree of Distribution (DD) of investigation elements were calculated by fractions C1, M1, and NC1.

The distribution of the elements was calculated using Equation (1):

$$DD_i = X_j C_{ij} / C_i \quad (1)$$

where:

DD_i—the degree of distribution of the "*i*-th" element;
X_j—the weight fraction of "*j*-th" fraction in products;
C_{ij}—the weight concentration of the "*i*-th" element in the "*j*" fraction;
C_i—the weight concentration of the "*i*-th" element in the sample.

2.10. Thermogravimetric Analysis of the Sample

The nonisothermal thermogravimetric curve (Tg) of the pyrolyzed NC2 fraction was recorded on the LECO TGA 701 thermogravimetric analyzer. Tg curve recordings were performed under the following conditions: sample weight of 0.5 g, crucible of aluminum oxide (Al_2O_3), in the temperature range from 25 to 800 °C, heating rate of 10 °C min^{-1}, with nitrogen flow of 100 cm^3 min^{-1}.

2.11. Vacuum Pyrolysis

Vacuum pyrolysis of the sample was performed using the setup schematically presented in Figure 1.

Pyrolysis was performed in a laboratory pyrolytic reactor with a "fixed bed". The sample was measured and placed in a special quartz vessel. The reactor was purged with nitrogen at a flow rate of Q = 80 mL min^{-1} until O_2 was removed. After removing O_2 from the reactor system, the reactor was connected to a vacuum pump, heated at a constant heating rate of v = 10 °C min^{-1} to 550 °C, and maintained at that temperature

for 120 min. In order to determine the volume of gas products of pyrolysis at the end of the system, a cumulative flow meter was fixed, which measured the volume of formed gases. The volatiles released were introduced into a condenser (1 M NaOH solution); then, the condensable gas condensate and HBr were absorbed in the condenser, and then non-condensable gases were collected in the gas bag for further analysis. The separated pyrolytic oil in the condensate was separated from the aqueous phase, dried, and weighed. The quartz vessel (pyrolysis residue) was removed from the reactor and cooled to room temperature. The pyrolytic residue was separated from the quartz vessel and its mass was measured. The carbon content in the residue was determined using the elemental analyzer EMIA 920 HORIBA (HORIBA Ltd., Kyoto, Japan). The concentration of MEs and EROs (elements refractory oxides) was determined by the XRF method, and the concentration of REEs was determined by ICP coupled by mass spectrometry.

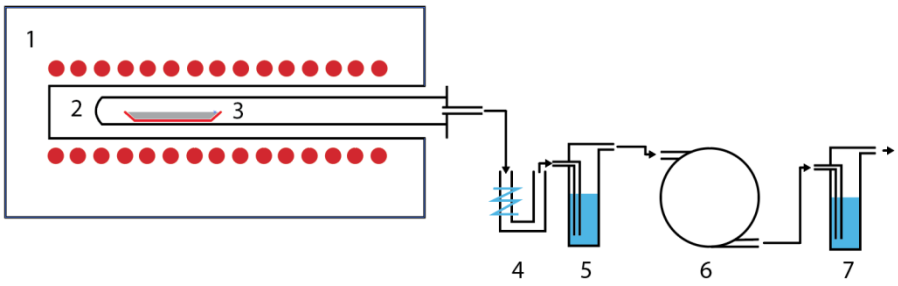

Figure 1. Experimental setup: 1. electro-resistant furnace; 2. quartz tube; 3. sample; 4. cooling of the pyrolysis oil; 5. gas purification through 1 M NaOH; 6. vacuum pump; 7. gas purification after vacuum pump.

2.12. Chemical Composition of Gas Pyrolytic Fraction and Pyrolytic Oil

The chemical composition of the gaseous fraction was determined by the gas chromatographic method. Gas chromatograms were recorded on a gas chromatograph coupled with mass spectroscopy, GC/MS, Shimadzu QP2010 SE, model HP 5890/5970 (Shimadzu Corporation, Kyoto, Japan). Mass spectra were optimized with an electronic ionizer at 70 eV, at a temperature of ~180 °C.

The chemical composition of the separated and collected pyrolytic oil was analyzed and determined by the chromatographic method. The prepared sample was dried at room temperature and analyzed on a gas chromatograph coupled with mass spectroscopy (GC/MS). A slightly polarized silicon capillary column 30 mm long and 0.25 mm in diameter was used (Varian VF1 MS with coating 1 µm). The injector temperature was 200 °C, the split flow was 14:1, and the column flow was controlled with He (5.0 purity).

3. Results and Discussion

The electrostatic separation of raw materials results in the formation of three fractions: conductive (C1), mixed (M1), and nonconductive (NC1). The average chemical composition of input materials entering the first ESS is shown in Table 1.

Table 1. Chemical composition of input materials.

Elements	Concentration
-	[wt.%]
Fe	0.540 ± 0.003
Cu	18.10 ± 0.03
Sn	1.00 ± 0.03
Pb	0.362 ± 0.006
Zn	1.13 ± 0.01
Ba	3.05 ± 0.02
Br	26.72 ± 0.03
Si	13.2 ± 0.2
Al	12.6 ± 0.5
Ca	8.00 ± 0.05

The weight fraction and bulk density products of electrostatic separation and bulk density fraction are shown in Table 2.

Table 2. Weight fraction and bulk density in ESS fractions.

Fraction	Weight Fraction	Bulk Density
-	[wt.%]	[kg·m^{-3}]
C1	15.0	950
M1	33.0	820
NC1	52.0	720

After the first ESS, NC1 has the largest weight share with 52 wt.%, while the weight share of fraction C1 is 15 wt.%. At the same time, the bulk density of the C1 fraction is the highest at 950 kg·m^{-3}, while the bulk density of the NC1 fraction is 720 kg·m^{-3}. The determined mass distribution by fractions indicates that ESS divides the elements MEs, Br, and EROs (elements contained in refractory oxides) and is closely related to the particle size distribution, which is shown in Table 3.

Table 3. Particle sizes distribution of ESS fractions.

Particle Sizes	ESS Fractions		
-	C1	M1	NC1
		weight	Fraction
[mm]		[wt.%]	
>4	8.45	54.85	49.04
2.0–4.0	51.92	42.58	10.77
0.5–1.00	21.68	1.54	35.05
0.25–0.5	17.14	1.03	5.03
0.125–0.250	0.64	0.00	0.11
0.1–0.125	0.15	0.00	0.00
0.063–0.100	0.02	0.00	0.00
0.036–0.063	0.00	0.00	0.00
<0.036	0.00	0.00	0.00
Sum	100.00	100.00	100.00

The relative contribution of fraction (C1) in the products is small and amounts to 15.0 (wt.%), but the bulk density of this fraction is highest. In the fraction (C1), particles with dimensions from 8 mm to 0.1 mm are present with the maximum share in the distribution of particles whose dimensions range from 2 to 4 mm, 51.9 (wt.%). In contrast, in the M1 fraction, particles with dimensions of 8–1 mm are present with a maximum proportion of particles with dimensions of 4–8 mm, 54.85 (wt.%). In the NC1 fraction, particles with dimensions of 8–0.25 mm are present with a maximum contribution of particles with

dimensions of 4–8 mm, 49.04 (wt.%). Figure 2 shows the XRF spectrum of the M1 fraction as an example.

As can be seen from Figure 2, the ESS fractions consist of a large number of metallic elements, MEs (Fe, Cu, Zn, Pb, Ba, Sn), elements contained in refractory oxides, EROs (Al, Ca, and Si), and Br. Considering a large number of identified elements for monitoring the influence of ESSs on the concentration of MEs, (Fe, Cu, Sn, Pb, Zn, Ba) were selected from EROs (Si, Al, Ca) and Br. Table 4 shows the chemical composition of fractions C1, M1, and NC1.

As a result of the ESS in the starting material, based on the presented results, the following occurs:

(a) Increase in the concentrations of Cu and Pb in C1 and M1 fractions, and decrease in the concentration in NC1 fraction;
(b) Increase in the concentrations of Br in NC1 fraction and decrease in the concentration of Br in C1 and M1;
(c) Increase in the concentration of Al in C1 fraction and decrease in its concentration in M1 and NC1;
(d) Complex distribution of other elements by phases. Concentrations of the REEs are shown in Table 5.

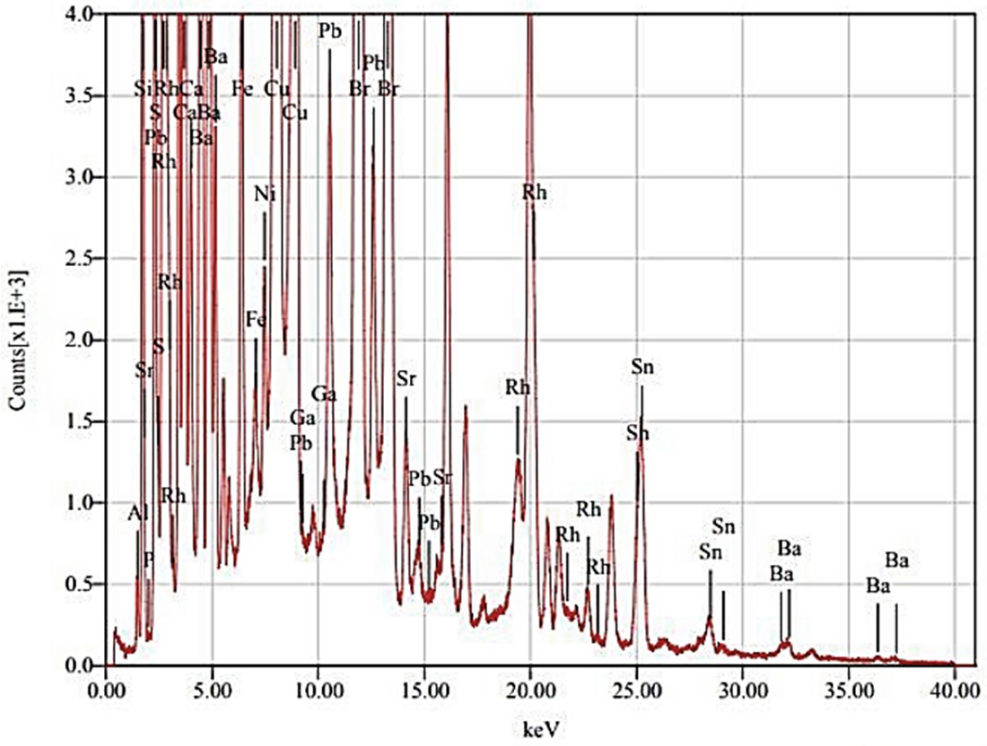

Figure 2. XRF spectra of the M1 fraction.

Table 4. Chemical composition of fractions C1, M1, and NC1.

Element	ESS Fraction		
-	C1	M1	NC1
-		[wt.%]	
Fe	0.292 ± 0.003	0.353 ± 0.003	0.731 ± 0.008
Cu	26.97 ± 0.03	35.62 ± 0.04	4.25 ± 0.01
Sn	0.92 ± 0.02	2.05 ± 0.03	0.37 ± 0.03
Pb	0.571 ± 0.005	0.626 ± 0.007	0.132 ± 0.005
Zn	3.76 ± 0.01	-	1.079 ± 0.007
Ba	0.65 ± 0.01	7.31 ± 0.03	1.04 ± 0.02
Br	1.272 ± 0.006	19.77 ± 0.03	38.49 ± 0.04
Si	3.1 ± 0.1	20.9 ± 0.3	11.2 ± 0.2
Al	57.2 ± 0.5	5.5 ± 0.7	4.3 ± 0.8
Ca	-	4.22 ± 0.04	12.70 ± 0.07

The concentration of rare-earth elements in the C1 fraction is 30.4 ppm, the most common element from the group of rare-earth elements in this fraction is Ce, and the elements La, Y, and Sc are present in lower concentrations. In the M1 fraction, the total content of rare-earth elements is approximately the same as in the C1 fraction, 39.9 ppm. The most common element from the group of rare-earth elements is Ce, and the elements La, Nb, and Y are also present in significant concentrations. The total concentration of elements from the group of rare-earth elements in the NC1 fraction is less than their content in the C1 and M1 fractions, and it is 24.5 ppm. The most common element from the group of rare-earth elements in the C1 and M1 fractions is Ce, and La and Nd are present in more significant concentrations. REEs from the C1 fraction could be recovered through standard metallurgical routes (e.g. by processing sludge from electrowinning process). Non-conductive fractions in practice are usually used to recover polymer materials, so REEs from this fraction will be lost unless it was used for pyrolysis for energy recovery.

Table 5. The concentration of REEs in fractions C1, M1, and NC1 *.

Element	Fractions			
-	**C1**	**M1**	**NC1**	**R**
-	**Concentration [ppm]**			
Sc	2.6 ± 0.2	2.4 ± 0.2	1.7 ± 0.1	0.07
Y	3.30 ± 0.07	4.00 ± 0.08	1.80 ± 0.04	0.02
La	4.40 ± 0.04	7.00 ± 0.07	4.30 ± 0.04	0.01
Ce	9.00 ± 0.01	13.10 ± 0.01	8.900 ± 0.001	0.001
Pr	1.10 ± 0.04	1.50 ± 0.05	0.9 ± 0.3	0.034
Nd	4.30 ± 0.02	5.4 ± 0.1	3.30 ± 0.07	0.02
Sm	0.880 ± 0.001	1.000 ± 0.001	0.580 ± 0.001	0.001
Eu	0.300 ± 0.001	0.420 ± 0.001	0.180 ± 0.001	0.001
Gd	0.760 ± 0.001	1.000 ± 0.061	0.560 ± 0.001	0.001
Dy	0.570 ± 0.001	0.740 ± 0.001	0.390 ± 0.001	0.001
Ho	0.110 ± 0.001	0.140 ± 0.001	0.080 ± 0.001	0.001
Er	0.270 ± 0.001	0.380 ± 0.001	0.190 ± 0.001	0.001
Yb	0.270 ± 0.001	0.420 ± 0.001	0.200 ± 0.001	0.001

* Elements with value less than 0.10 have not been taken to consideration.

Considering that the concentration of elements from the REE group is highest in the M1 fraction, this fraction was subjected to additional electrostatic separation. Also, additional separation is needed because the metal parts are firmly attached to the polymer matrix. The weight and bulk density fractions of the obtained ESS fractions are shown in Table 6.

Table 6. Weight fractions and bulk density of the ESS fractions.

Fraction	Fraction	Bulk Density
	[wt.%]	[kg·m^{-3}]
C2	11.0	1210
M2	29.0	820
NC2	60.0	480

After additional electrostatic separation of M1 fraction, the non-conductive (NC2) fraction increased share of 60%, while the share of the conductive (C2) decreased to 11.0%. Among ESS products, the C2 fraction has the highest bulk density of 1210 kg·m^{-3}, and NC2 has the lowest bulk density. Table 7 shows the particle size distribution of the products of the ESS M1 fraction.

Table 7. Particle sizes distribution of fractions C2, M2, and NC2 ESS.

Particle Sizes	Fractions		
-	C2	M2	NC2
[mm]		[wt.%]	
>4	0.56	0.00	0.00
2.0–4.0	27.53	36.62	6.00
1.0–2.0	34.35	58.14	26.95
0.5–1.00	22.85	2.82	24.05
0.25–0.5	11.74	0.58	18.00
0.125–0.250	2.50	0.51	10.02
0.1–0.125	0.22	0.31	1.98
0.063–0.100	0.12	0.41	4.00
0.036–0.063	0.07	0.20	3.20
<0.036	0.06	0.41	5.80
Sum	100.00	100.00	100.00

In the C2 fraction, particles with dimensions of 4–0.036 mm are present with a maximum contribution of particles with dimensions of 1–2 mm, 34.35 (wt.%). In the M2 and NC2 fractions, particles with dimensions of 4–0.036 mm are present with a maximum contribution of particles with dimensions of 1–2 mm, 58.14 (wt.%) and 26.95 (wt.%), respectively.

As can be seen from Figure 3, the ESS fraction NC2 consist of a large number of metallic elements, elements contained in refractory oxides, and Br. Considering a large number of identified elements for monitoring the influence of ESSs on the concentration of MEs, (Fe, Cu, Sn, Pb, Zn, Ba) were selected from EROs (Si, Al, Ca) and Br. Table 8 shows the chemical composition of fractions C2, M2, and NC2.

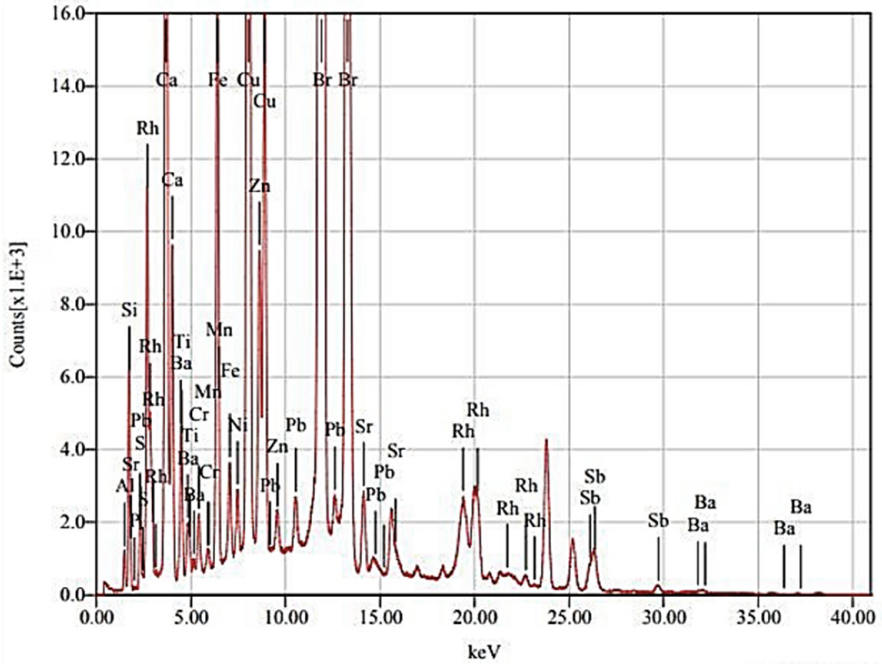

Figure 3. XRF spectrum of the NC2 fraction.

Table 8. Chemical compositions of C2, M2, and NC2 fractions.

Elements	Fractions		
-	C2	M2	NC2
-		[wt.%]	
Fe	0.174 ± 0.003	0.773 ± 0.007	1.64 ± 0.01
Cu	59.20 ± 0.05	12.29 ± 0.02	7.10 ± 0.02
Sn	2.51 ± 0.03	0.37 ± 0.03	-
Pb	1.61 ± 0.01	0.396 ± 0.006	0.247 ± 0.005
Zn	1.20 ± 0.01	0.185 ± 0.003	0.465 ± 0.004
Ba	1.62 ± 0.01	3.97 ± 0.03	1.40 ± 0.02
Br	4.52 ± 0.01	36.25 ± 0.04	32.25 ± 0.04
Si	5.2 ± 0.2	13.6 ± 0.2	22.0 ± 0.3
Al	20.7 ± 0.6	8.3 ± 0.8	9.2 ± 0.8
Ca	1.769 ± 0.02	12.10 ± 0.06	20.23 ± 0.07

Comparing the concentration of MEs, Br, and EROs in the M1 fraction, there is (a) an increase in the concentration of Zn and Al in all fractions, (b) an increase in the concentration of Fe and Ca in M2 and NC2 fractions, (c) an increase in the concentration of Br in M2 and NC2 fractions, (d) a decrease in the concentration of Cu in M2 and NC2 fractions, and (e) complex changes in concentrations of other elements by fractions. Table 9 shows the concentration of REEs in fractions C2, M2, and NC2.

Table 9. The concentration of REEs in fractions C2, M2, and NC2 *.

Elements	ESS Fractions		
	C2	**M2**	**NC2**
	Concentration	**[ppm]**	
Sc	0.44 ± 0.03	2.7 ± 0.2	3.5 ± 0.2
Y	1.23 ± 0.02	5.1 ± 0.1	19.4 ± 0.4
La	3.75 ± 0.04	7.70 ± 0.08	10.1 ± 0.1
Ce	4.720 ± 0.004	15.40 ± 0.01	16.90 ± 0.02
Pr	1.89 ± 0.06	1.80 ± 0.06	2.9 ± 0.1
Nd	39.2 ± 0.8	6.9 ± 0.1	20.9 ± 0.4
Sm	1.870 ± 0.002	1.300 ± 0.001	3.700 ± 0.004
Eu	0.750 ± 0.001	0.400 ± 0.001	1.500 ± 0.002
Gd	3.780 ± 0.004	1.200 ± 0.001	2.300 ± 0.002
Dy	0.850 ± 0.001	0.850 ± 0.001	0.860 ± 0.001
Ho	0.600 ± 0.001	0.410 ± 0.001	0.420 ± 0.001
Er	0.280 ± 0.001	0.410 ± 0.001	0.420 ± 0.001
Yb	0.130 ± 0.001	0.360 ± 0.001	0400 ± 0.001
U	0.360 ± 0.004	1.000 ± 0.001	1.000 ± 0.001

* Elements with value less than 0.10 have not been taken to consideration.

The total content of the elements from the group of rare-earth elements in fraction C2 is 59.85 ppm. The most common element from the group of rare-earth elements is Nd (39.2 ppm), and Ce and La (4.7 and 3.8 ppm, respectively) are present in more significant concentrations. In the M2 fraction, the total content of elements from the group of rare-earth elements is lower than in the C2 fraction, and it is 47.6 ppm. The most common element in the M2 fraction is Ce (15.4 ppm), and La, Nd, and Y (7.7, 6.9, and 5.1 ppm, respectively) are present in more significant concentrations. The total concentration of elements from the group of rare-earth elements in the non-conductive (NC2) dusty fraction is 85 ppm, and it is significantly higher than the concentration of rare-earth elements in the C2 and M2 fractions. The most common elements from the group of rare-earth elements in this fraction are Nd, Y, and Ce (20.9, 19.4, and 16 ppm, respectively), and La and Sc (10, 3.5 ppm, respectively) are present in significant concentrations.

Based on determining values of weight fractions of individual fractions in ESS products and concentrations of MEs, Br, EROs, and REEs in them, it can be assumed that ESS leads to a significant redistribution of elements contained in the raw material by fractions. Table 10 shows the calculated distribution of elements by fractions C1, M1, and NC1

Table 10. Distribution of elements by fractions C1, M1, and NC1.

Element	ESS Fraction		
-	**C1**	**M1**	**NC1**
-		**DD**	
		[wt.%]	
Fe	8.2	21.1	70.7
Cu	22.3	65.4	12.3
Sn	13.3	67.4	19.3
Pb	23.7	57.1	19.2
Zn	49.8	0.0	50.2
Ba	3.1	79.3	17.6
Br	0.9	24.5	74.6
Si	3.5	52.3	44.2
Al	67.6	14.6	17.8
Ca	0.0	17.4	82.6

Metal elements Cu, Sn, Pb, and Ba are distributed predominantly in the M1 fraction, while Fe and Zn are distributed in the NC1 fraction. Br is also predominantly distributed

in the NC1 fraction, while EROs are differentiated and redistributed by fractions. Ca is predominantly distributed in the NC1 fraction, Al in the C1 fraction, and Si in the M1 fraction. The obtained redistribution of elements does not follow the expected distribution of elements by fractions in the case of the application of ESS, and indicates a significant influence of the phase and granulometric composition of the raw material on the distribution of the ESS products. Table 11 shows the calculated degrees of distribution of elements from the group of rare-earth elements.

Table 11. Distribution of elements from the group of REEs.

Elements	ESS Fraction		
-	C1	M1	NC1
-		DD	
		[%]	
Sc	7.3	32.4	60.3
Y	17.3	47.8	34.9
La	12.0	45.0	43.0
Ce	12.9	42.1	45.0
Pr	14.8	33.2	52.0
Nd	15.2	43.1	41.7
Sm	17.1	43.4	39.5
Eu	15.9	49.0	35.1
Gd	16.1	44.2	39.7
Tb	16.2	32.1	51.7
Dy	15.5	46.0	38.5
Er	15.4	50.0	34.6
Yb	16.1	45.1	38.8
Th	1.1	21.1	77.8

Based on the results shown in Table 11, it can be concluded that the elements Y, La, Nd, Sm, Eu, Gd, Dy, and Er are predominantly redistributed in the M1 fraction, and elements Sc, Ce, Pr, Tb, and Th are redistributed in the NC1 fraction.

The determined redistribution of REEs by fractions of ESS also significantly deviates from the expected distribution of REEs by fractions based on which the implemented NC1 fraction should be enriched with elements from the REE group that have high surface charge and high current conductivity. To determine the influence of ESS on the redistribution of elements from the M1 fraction, the degrees of distribution of MEs, Br, and EROs were calculated. Table 12 shows the calculated degrees of distribution of elements by fractions.

Metal elements Cu, Sn, and Pb are predominantly distributed in the C2 fraction. Fe and Zn are distributed in the NC2 fraction, while Ba is distributed in the M2 fraction. EROs and Br are predominantly distributed in the NC2 fraction.

The obtained redistribution of elements also deviates significantly from the expected redistribution of elements caused by the action of the electrostatic field based on the inability to accumulate surface charges and electric current conductivity and is most likely due to the ability of large grains to combine with metal, plastic, and refractory material, and thus reduce the efficiency of ESS.

Table 13 shows the degrees of distribution of elements from the group of rare-earth elements by fractions.

As can be seen from Table 13, all elements from the REE group are redistributed in NC2, which is a new and completely unexpected result, the explanation of which requires several additional investigations.

Table 12. Distribution of elements by fractions C2, M2, and NC2.

Elements	ESS Fraction		
-	C2	M2	NC2
-		DD	
		[%]	
Fe	2.9	31.4	65.7
Cu	47.2	24.1	28.7
Sn	74.0	25.3	0.0
Pb	42.2	24.4	32.9
Zn	29.8	10.64	59.6
Ba	0.9	54.7	40.1
Br	1.2	34.6	63.7
Si	3.4	22.1	74.4
Al	24.0	24.2	55.0
Ca	1.3	22.2	76.6

Table 13. Distribution of elements from the group of rare-earth elements.

Elements	ESS Fraction		
-	C2	M2	NC2
-		DD	
		[%]	
Sc	1.8	26.9	72.41
Y	0.2	11.5	91.80
La	0.5	26.5	72.28
Ce	3.7	30.0	65.78
Pr	8.9	21.0	68.54
Nd	24.2	10.5	66.00
Sm	7.9	13.2	78.57
Eu	7.2	14.5	81.81
Gd	21.0	14.3	66.66
Tb	3.4	9.8	86.44
Dy	12.5	25.0	63.75
Er	5.5	26.3	65.78
Yb	2,9	28.6	68.57

Pyrolysis of waste electronic material is an environmentally friendly, energy-efficient waste treatment technique to convert it into other products. During the pyrolysis process, the materials contained in the electronic waste are converted into flammable gases, pyrolytic oil, and solid residue. Pyrolytic oil and flammable gases can be used as energy sources [28]. The solid residue formed during pyrolysis is enriched with metals and fiber glass contained in electronic waste and carbon, which facilitates the recuperation of metals from electronic waste. With this in mind, and to further concentrate metals and elements from REEs, the NC2 fraction (with the highest content of REEs) was subjected to a pyrolysis process. As, due to the particle size composition of the raw material, energy consumption in the implementation of the pyrolysis process is primarily determined by the temperature at which the pyrolysis is performed [32,33]. Figure 4 shows the TG and DTG curves of the pyrolysis of the NC2 fraction. To determine the optimal pyrolysis temperature, a non-isothermal thermogravimetric curve of the pyrolysis of the NC2 fraction was recorded. Figure 3 shows the TG and DTG curves of the pyrolysis of the NC2 fraction.

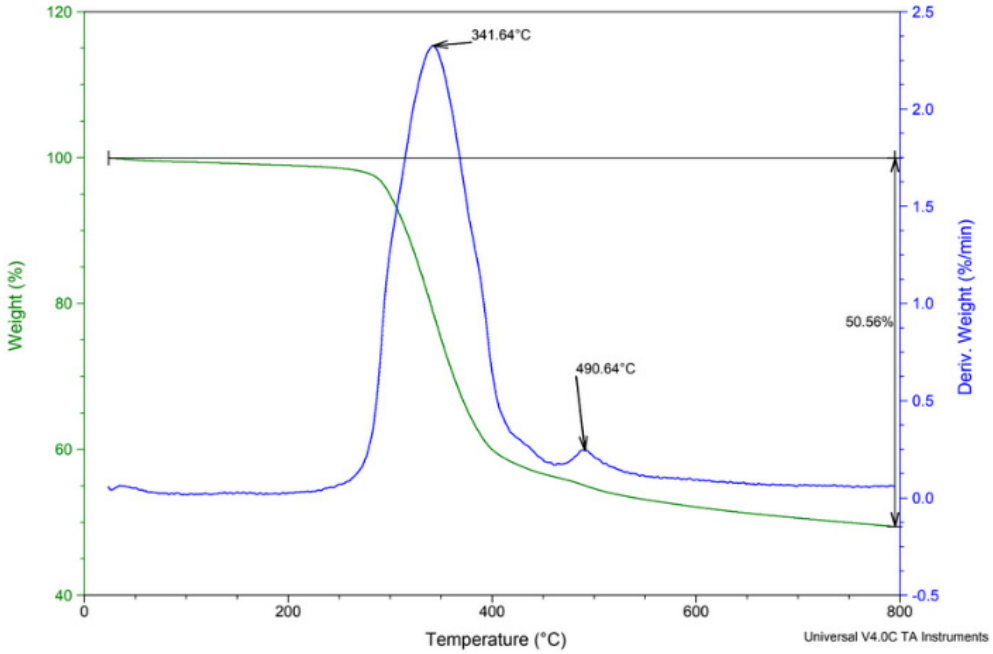

Figure 4. TG and DTG curves of the pyrolysis of the NC2 fraction.

As can be seen from Figure 3, thermal degradation of the NC2 fraction takes place in the temperature range from T = 25 °C to T = 800 °C with a weight loss of 51%. The maximum degradation rate is reached at T = 342 °C. On the TG and DTG curves, three separate stages of the thermal NC2 fraction are observed. The first degradation stage takes place in the temperature range from T = 25 °C to T = 250 °C and is followed by a weight loss of 2.2%.

The main degradation stage of the NC2 fraction takes place in the temperature range from T = 250 °C to T = 465 °C with a weight loss of 39.2%. The third degradation stage of the NC2 fraction begins to take place at T = 465 °C and is followed by a weight loss of 9.3%. Considering the shape of the TG curve, we found that the temperature for low-temperature vacuum pyrolysis is 550 °C, to ensure complete pyrolysis.

The distribution of pyrolysis products of the NC2 fraction is shown in Table 14.

Table 14. Distribution of the pyrolysis products of NC2 fraction.

Product	Weight Fraction
-	[wt.%]
Gas	10.2
Pyrolytic oil	35.4
M + NM phase	45.1
Carbon	9.3

The most common pyrolysis product is the M + NM phase with a percentage of 45.1%. The percentage of pyrolytic oil is significant and amounts to 35.4%, while the percentages of the gas phase (10.2%) and carbon (9.3%) are relatively small.

SEM analysis is used to represent the morphology and structure of NC2—dust fraction: (coarse and fine grinding mix. PCB, magnetic separation, and double separation on an electrostatic separator, Hamos Germany). Figure 5 shows Sample NC2—dust: (a) before and (b) after vacuum pyrolysis.

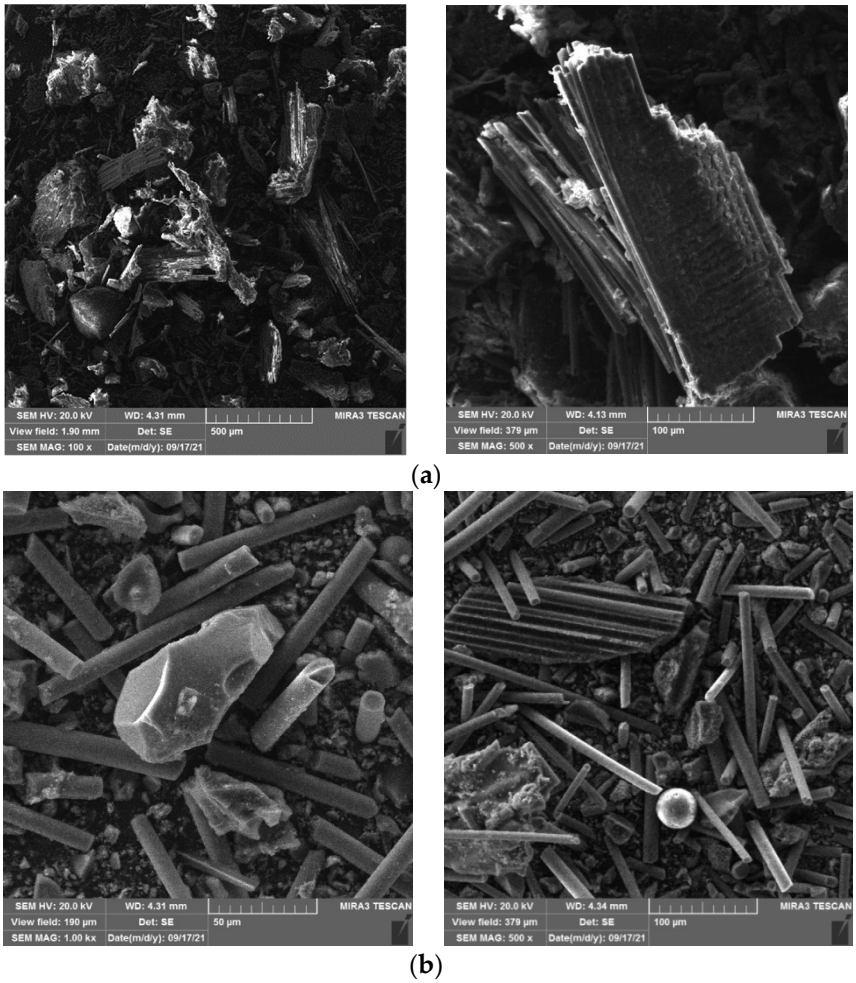

Figure 5. (**a**) NC2—dust from mechanical treatment before vacuum pyrolysis, and (**b**) NC2—dust from mechanical treatment after vacuum pyrolysis, at different magnifications.

Figure 5a clearly shows the presence of the organic phase collected in a large piece of light paints, and then glass fibers of the claviform structure and plastic particles that are of regular shape. Metals are seen as irregular shiny shapes. Figure 5b shows the formed forms after treatment of the NC2 fraction by low-temperature pyrolysis. The images show that the forms are free of organic matter, the fiber glass is properly broken in the form of a broken rod, the amount of carbon is significantly reduced, while metals such as REEs are concentrated in larger and smaller groups of irregular shape. The presence of metals in the sample after low-temperature vacuum pyrolysis is a consequence of the impossibility of proper comminution of thin metal conductors. In such a form, REEs could be transferred to metallurgical processing for recovery, even to a greater extent than described in the literature—only by electrostatic separation [34].

Non-isothermal thermogravimetric pyrolysis of the NC2 fraction takes place in three degradation stages. The first degradation stage is most likely associated with the decomposition of products containing H_2O and CO_2 and is associated with the glass transition of brominated epoxy resins (BERs) [35].

In the two degradation stages, the structure of the NC2 fraction is destroyed due to BER decomposition. The BER of the decomposition process is complex. Following the works of Evangelopoulos and Gruse, it begins with the decomposition of brominated flame retardants (BFRs) contained in BER, accompanied by the release of HBr and the generation of tetrabromobisphenol A (TBBPA) and bisphenol A (BPA). Further decomposition of TBBPA and BPA [36] leads to the formation of brominated aromatics. The complete

decomposition of BER (brominated epoxy resin) with polycondensation gasification of aromatic components leads to the formation of carbonaceous materials (tar).

The third degradation stage of the NC2 fraction is most likely related to the decomposition of carbon materials in the solid residue [37].

Based on the results obtained during the examination of nonisothermal thermal degradation of the NC2 fraction, its pyrolysis was performed at T = 550 °C. The chemical composition of the gas phase is shown in Table 15.

Table 15. Chemical composition of the gas phase.

Component	Concentration
	[wt.%]
H_2	7.9
CO	28.6
CO_2	50.6
CH_4-C_4H_{10}	11.8
CH_3Br	1.1

The most common component of the gas phase formed by pyrolysis of the NC2 fraction is CO_2 with a content of 50.6 (wt.%). The CO content in the gas phase is significant and amounts to 28.6 (wt.%). The mass fraction of fuel gases (H_2 and CH_4-C_4H_{10}) is at the level of 19.7 (wt.%), and the content of CH_3Br is 1.1 (wt.%). Table 16 shows the chemical composition of pyrolytic oil.

Table 16. Chemical composition of pyrolytic oil.

Chemical Compound	Concentration
	[wt.%]
Phenol	38.0
4-(1-metiletil)phenol	23.8
m-ethylphenol	6.9
p-methylphenol	5.7
o-bromophenol	4.3
m-izo-propylphenol	3.5
Acetone	2.7
2-metil-2,3-dihydrobenzofuran	2.2
2-methyl-benzofuran	1.9
1-hidroksi-2.4-dibrombenzen	1.6
o-ethylphenol	1.5
2-(1-methylethyl)phenol	1.5
Toluen	1.2
Benzofuran	1.20
p-ethylphenol	1.2
Benzophenone	1.0
2.3-dimethyl-benzofuran	1.0
2.6-Dibromphenol	1.0

As can be clearly seen from Table 16, the heads are components of pyrolytic oil with a weight concentration dominating in pyrolytic oil with 38.0 wt.% and 23.8 wt.%, respectively, by fractions of phenol and 4-(1-methylethyl) phenol.

The chemical composition (M + NM) of the pyrolytic solid residue phase is shown in Table 17.

Table 17. Chemical composition (M + NM) of the pyrolytic solid residue phase.

Element	Concentration
	[wt.%]
Fe	3.01 ± 0.02
Cu	13.10 ± 0.03
Pb	0.512 ± 0.005
Zn	0.910 ± 0.005
Ba	2.60 ± 0.03
Al	17.01 ± 0.49
Si	40.81 ± 0.51
Ca	22.82 ± 0.06

The most represented metal in the (M + NM) phase of the solid residue is Cu with 13.1 (wt.%), which is significantly higher than their concentration in the NC2 fraction. Fe is present in this phase at the concentration 3.0 wt.%, while the concentrations of other examined metals are less than 1 wt.%. The concentration of Si in this pyrolysis product is a maximum of 40.8 wt.% and is significantly higher than its concentration in the NC2 fraction.

Table 18 shows the concentrations of REEs in the (M + NM) phase of the solid residue.

Table 18. Concentrations of REEs in the (M + NM) phase of the solid residue.

Element	Concentration
	[ppm]
Sc	6.51 ± 0.60
Y	35.90 ± 0.20
La	18.72 ± 0.15
Ce	31.30 ± 0.02
Pr	5.43 ± 0.01
Nd	38.72 ± 0.20
Sm	6.81 ± 0.01
Eu	2.84 ± 0.01
Gd	4.22 ± 0.01
Dy	1.720 ± 0.001
Ho	0.40 ± 0.01
Er	0.40 ± 0.01
Yb	0.40 ± 0.001
U	1.90 ± 0.01

The total concentration of REEs in (M + NM) is 200.27 ppm and it is about 90% higher than their total concentration in the NC2 fraction. Concentrations of elements Nd (38.72 ppm), Y (35.90 ppm), and Ce (31.30 ppm) are highest at this stage of the pyrolytic product. Elements from the rare-earth groups La (18.72 ppm), Sc (6.51 ppm), and Sm (6.81 ppm) are present in significant concentrations in the (M + NM) phase. The concentrations of other elements from the group of rare-earth elements are low.

A high contribution of pyrolytic oil and (M + NM) solid residue phase with an increased concentration of metals and elements from the group of rare-earth elements indicates that the combination of adequate mechanical preparation of waste electronic materials and electrostatic separation coupled with low-temperature vacuum pyrolysis is a highly efficient technique for obtaining energy sources (combustible gases, pyrolytic oil, and carbon), metals, and REEs.

4. Conclusions

Considering the results obtained in this paper and the main objectives of this paper, it can be concluded that ESS leads to a significant distribution of elements contained in the raw material by separation products; MEs (Cu, Sn, and Pb) and REEs are predominantly distributed in the M1 fraction, and Br is distributed in the NC1 fractions. The subsequent

ESS M1 fraction leads to a new distribution of elements due to MEs distributed in the C2 fraction, and Br, EROs, and REEs in the NC2 fraction. The maximum concentration of REEs was achieved in the NC2 fraction. The optimum temperature for vacuum pyrolysis of the NC2 fraction is T = 550 °C. The dominant products of vacuum pyrolysis are M + MN phases and pyrolytic oil. The concentration of REEs in the M + NM phase enables the economically viable production of REEs from e-waste.

Author Contributions: Research concept, V.M., Ž.K. and A.P.; data curation, A.P. and J.P.; formal analysis, J.P.; investigation, V.M., M.R. and A.P.; methodology, J.P. and M.R.; project administration, A.P.; resources, A.P.; supervision, B.A. and Ž.K.; validation, B.A. and J.P.; writing—original draft, A.P.; writing—review & editing, V.M., B.A. and M.R. All authors have read and agreed to the published version of the manuscript.

Funding: Funding for the publication was contributed by the author Andjelka Popović, during the preparation of her doctoral dissertation.

Institutional Review Board Statement: Not applicable.

Informed Consent Statement: Not applicable.

Data Availability Statement: Data sharing not applicable.

Acknowledgments: (1) For assistance in the material and use of devices and equipment to the operator for IT waste recycling "Alkemica Solutions", Novi Sad, Serbia. (2) JEOL, Germany, for making XRF spectra and chemical composition of the analyzed samples on JSX-1000S X-ray fluorescence spectrometer (XRF) manufactured by JEOL, Germany. (3) INSTITUTE OF MINING AND METALLURGY BOR Laboratory for Chemical Testing-HTK, from Bor for the analysis of REEs on the instrument of analysis on a mass spectrometer with inductively coupled plasma (ICP-MS Agilent 7500), I Tg analysis on LECO TGA 701 thermogravimetric analyzer.

Conflicts of Interest: The authors declare no conflict of interest.

References

1. Balaram, V. Rare earth elements: A review of applications occurrence exploration analysis recycling and environmental impact. *Geosci. Front.* **2019**, *10*, 1285–1303. [CrossRef]
2. Costis, S.; Mueller, K.K.; Coudert, L.; Neculita, C.M.; Reynier, N.; Blais, J.-F. Recovery potential of rare earth elements from mining and industrial residues: A review and cases studies. *J. Geochem. Explor.* **2021**, *221*, 106699. [CrossRef]
3. Van Gosen, B.; Verplanck, P.; Long, K.; Gambogi, J.; Seal, R. *The Rare-Earth Elements—Vital to Modern Technologies and Lifestyles*; Fact Sheet 2014–3078; U.S. Geological Survey: Reston, VA, USA, 2014; pp. 1–4. Available online: https://pubs.usgs.gov/fs/2014/3078/pdf/fs2014-3078.pdf (accessed on 30 April 2022).
4. Pandey, B.D.; Abhilash; Meshram, P. An Overview of the Recent Status of Critical and Strategic Metal Production and Development in India. In *Critical and Rare Earth Elements: Recovery from Secondary Resources*; Abhilash, Akcil, A., Eds.; CRC Press: Boca Raton, FL, USA; Taylor & Francis Group LLC: London, UK; New York, NY, USA, 2019; pp. 1–36.
5. Dushyant, N.; Batapola, N.; Ilankoon, I.; Rohitha, S.; Premasiri, R.; Abeysinghe, B.; Ratnayake, N.; Dissanayake, K. The story of rare earth elements (REEs): Occurrences global distribution genesis geology mineralogy and global production. *Ore Geol. Rev.* **2020**, *122*, 103521. [CrossRef]
6. Gupta, C.K.; Krishnamurthy, N. *Extractive Metallurgy of Rare Earths*; CRC Press: Boca Raton, FL, USA; London, UK; New York, NY, USA; Washington, DC, USA, 2005; pp. 1–132.
7. Terry, F. 2019 Rare Earths Rarely So Strategic. Semicond. Dig. Available online: https://www.semiconductor-digest.com/2019-rare-earths-rarely-so-strategic/ (accessed on 30 April 2022).
8. Mancheri, N.A.; Sprecher, B.; Bailey, G.; Ge, J.; Tukker, A. Effect of Chinese policies on rare earth supply chain resilience. *Resour. Conserv. Recycl.* **2019**, *142*, 101–112. [CrossRef]
9. U.S. Geological Survey. *Mineral Commodity Summaries 2022*; U.S. Geological Survey: Reston. VA, USA, 2022; pp. 134–135. [CrossRef]
10. Forti, V.; Balde, C.P.; Kuehr, R.; Bel, G. *The Global E-Waste Monitor 2020: Quantities, Flows and the Circular Economy Potential*; United Nations University: Bonn, Germany; United Nations Institute for Training and Research: Geneva, Switzerland; International Telecommunication Union and International Solid Waste Association: Rotterdam, The Netherlands, 2020; pp. 1–120. Available online: https://ewastemonitor.info/gem-2020/ (accessed on 30 April 2022).
11. Van Yken, J.; Boxall, N.J.; Cheng, K.Y.; Nikoloski, A.N.; Moheimani, N.R.; Kaksonen, A.H. E-Waste Recycling and Resource Recovery: A Review on Technologies. Barriers and Enablers with a Focus on Oceania. *Metals* **2021**, *11*, 1313. [CrossRef]

12. Ogunniyi, I.O.; Vermaak, M.K.G.; Groot, D.R. Chemical composition and liberation characterization of printed circuit board comminution fines for beneficiation investigations. *Waste Manag.* **2009**, *29*, 2140–2146. [CrossRef] [PubMed]
13. Luda, M.P. Recycling of Printed Circuit Boards. In *Integrated Waste Management 2*; Kumar, M.S., Ed.; IntechOpen: London, UK, 2011.
14. Kumar, A.; Holuszko, M.; Espinosa, D.C.R. E-waste: An overview on generation, collection, legislation and recycling practices. *Resour. Conserv. Recycl.* **2017**, *122*, 32–42. [CrossRef]
15. Kumar, A.; Holuszko, M.E.; Janke, T. Characterization of the non-metal fraction of the processed waste printed circuit boards. *Waste Manag.* **2018**, *75*, 94–102. [CrossRef]
16. Duan, H.; Hu, J.; Yuan, W.; Wang, Y.; Yu, D.; Song, Q.; Li, J. Characterizing the environmental implications of the recycling of non-metallic fractions from waste printed circuit boards. *J. Clean. Prod.* **2016**, *137*, 546–554. [CrossRef]
17. Dylan, T.B.; Zyaykina, N.N.; Spencer, C.A.; Lawson, E.; Ploss, M.N.; Hua, I. Comprehensive elemental analysis of consumer electronic devices: Rare earth precious and critical elements. *Waste Manag.* **2020**, *103*, 67–75. [CrossRef]
18. Gaustad, G.; Williams, E.; Leader, A. Rare earth metals from secondary sources: Review of potential supply from waste and by products. *Resour. Conserv. Recycl.* **2021**, *167*, 105213. [CrossRef]
19. Jha, M.K.; Kumari, A.; Panda, R.; Kumar, J.R.; Yoo, K.; Lee, J.Y. Review on hydrometallurgical recovery of rare earth metals. *Hydrometallurgy* **2016**, *165*, 2–26. [CrossRef]
20. Tanaka, M.; Oki, T.; Koyama, K.; Narita, H.; Oishi, T. Recycling of rare earths from scrap. In *Handbook on the Physics and Chemistry of Rare Earths*; Bunzli, J.C.G., Pecharsky, V.K., Eds.; Elsevier: Amsterdam, The Netherlands, 2013; Volume 43, pp. 159–212.
21. Kaya, E.E.; Kaya, O.; Stopic, S.; Gürmen, S.; Friedrich, B. NdFeBMagnets Recycling Process: An Alternative Method to Produce Mixed Rare Earth Oxide from ScrapNdFeB Magnets. *Metals* **2021**, *11*, 716. [CrossRef]
22. Ma, Y.; Stopic, S.; Gronen, L.; Obradovic, S.; Milivojevic, M.; Friedrich, B. Neural network modelling for the extraction of rare-earth elements from eudialyte concentrate by dry digestion and leaching. *Metals* **2018**, *8*, 267. [CrossRef]
23. Demol, J.; Ho, E.; Senanayake, G. Sulfuric acid baking and leaching of rare earth elements, thorium and phosphate from a monazite concentrate: Effect of bake temperature from 200 to 800. *Hydrometallurgy* **2018**, *179*, 254–267. [CrossRef]
24. Stopic, S.; Friedrich, B. Leaching of rare earth elements from bastnasite ore (third part). *Mil. Tech. Cour.* **2019**, *67*, 561–572. [CrossRef]
25. Zhang, P.W.; Yokoyama, T.; Itabashi, O.; Wakui, Y.; Suzuki, T.M.; Inoue, K. Hydrometallurgical process for recovery of metal values from spent nickel metal hydride secondary batteries. *Hydrometallurgy* **1998**, *50*, 61–75. [CrossRef]
26. Liu, Z.; Li, M.; Hu, Y.; Wang, M.; Shi, Z. Preparation of large particle rare earth oxides by precipitation with oxalic acid. *J. Rare Earths* **2008**, *26*, 158–162. [CrossRef]
27. Arrachart, G.; Couturier, J.; Dourdain, S.; Levard, C.; Pellet-Rostaing, S. Recovery of RareEarth Elements (REEs) Using IonicSolvents. *Processes* **2021**, *9*, 1202. [CrossRef]
28. Chen, Y.; Liang, S.; Xiao, K.; Hu, J.; Hou, H.; Liu, B.; Deng, H.; Yang, J. A cost-effective strategy for metal recovery from waste printed circuit via crushing pre-treatment combined with pyrolysis: Effects of particle size and pyrolysis temperature. *J. Clean. Prod.* **2021**, *280*, 124505. [CrossRef]
29. Quan, C.; Li, A.; Gao, N. Synthesis of carbon nanotubes and porous carbons from printed circuit board waste pyrolysis oil. *J. Hazard. Mater.* **2010**, *179*, 911–917. [CrossRef] [PubMed]
30. Khanna, R.; Ellamparuthy, G.; Cayumil, R.; Mishra, S.K.; Mukherjee, P.S. Concentration of rare earth elements during high temperature pyrolysis of waste printed circuit boards. *Waste Manag.* **2018**, *78*, 602–610. [CrossRef] [PubMed]
31. Khanna, R.; Park, M.; Mukherjee, P.S.; Mishra, S.K.; Biswal, S.K.; Cayumil, R. Environmentally and Economically Sustainable Recovery of Precious Metals and Rare Earth Elements from Waste Printed Circuit Boards. In *Critical and Rare Earth Elements: Recovery from Secondary Resources*; Abhilash, Akcil, A., Eds.; CRC Press: Boca Raton, FL, USA; Taylor & Francis Group LLC: London, UK; New York, NY, USA, 2019; pp. 299–312, (In Indian). [CrossRef]
32. Chen, B.; He, J.; Sun, X.; Zhao, J.; Jiang, H.; Zhang, L. Separating and recycling metal mixture of pyrolyzed waste printed circuit boards by a combined method. *Waste Manag.* **2020**, *107*, 113–120. [CrossRef] [PubMed]
33. Guo, X.; Qin, F.; Yang, X.; Jiang, R. Study on low-temperature pyrolysis of large size printed circuit boards. *J. Anal. Appl. Pyrol.* **2014**, *105*, 151–156. [CrossRef]
34. Suponik, T.; Franke, D.M.; Nuckowski, P.M.; Matusiak, P.; Kowol, D.; Tora, B. Impact of Grinding of Printed Circuit Boards on the Efficiency of Metal Recovery by Means of Electrostatic Separation. *Minerals* **2021**, *11*, 281. [CrossRef]
35. Li, J.; Duan, H.; Yu, K.; Wang, S. Interfacial and mechanical property analysis of waste printed circuit boards subject to thermal shock. *J. Air Waste Manag. Assoc.* **2010**, *60*, 229–236. [CrossRef]
36. Cui, Q.; Li, R.; Gao, R.; Dan, R. Characterization of products recycling from PCB waste pyrolysis. *J. Anal. Appl. Pyrol.* **2010**, *89*, 102–106.
37. Chen, Y.; Yang, J.; Zhang, Y.; Liu, K.; Liang, S.; Xu, X.; Hu, J.; Yao, H.; Xiao, B. Kinetic simulation and prediction of pyrolysis process for non-metallic fraction of waste printed circuit boards by discrete distributed activation energy model compared with is conversional method. *Environ. Sci. Pollut. Res.* **2018**, *25*, 3636–3646. [CrossRef]